Enhanced tunability and linewidth sharpening of plasmon resonances in hybridized metallic ring/disk nanocavities

Feng Hao and Peter Nordlander*
Laboratory for Nanophotonics, Department of Physics and Astronomy, M. S. 61, Rice University, Houston, Texas 77005-1892, USA

Mathew T. Burnett
Centre for Photonics and Photonic Materials, Department of Physics, University of Bath, Bath BA2 7AY, United Kingdom

Stefan A. Maier†
Centre for Photonics and Photonic Materials, Department of Physics, University of Bath, Bath BA2 7AY, United Kingdom and Experimental Solid State Group, Physics Department, Imperial College, London SW7 2AZ, United Kingdom‡
(Received 23 July 2007; published 18 December 2007)

Using the finite-difference time-domain method, we investigate the plasmonic mode spectrum of a metallic nanostructure consisting of a concentric arrangement of a solid disk and a surrounding ring. We demonstrate that the energies of the plasmon modes depend sensitively on the structural parameters of the disk and the ring. We show that the nature of the plasmon modes can be understood simply as a hybridization of individual disk and ring plasmons. This interaction results in a redshifted bonding plasmon resonance of significantly narrower linewidth and larger electromagnetic field enhancements than the parent plasmons. This highly tunable nanostructure has significant potential as a substrate for surface enhanced spectroscopies.

DOI: 10.1103/PhysRevB.76.245417 PACS number(s): 71.45.Gm

The investigation of the spectral tunability of localized plasmon resonances in small metallic nanostructures has attracted a considerable amount of research effort in the field of plasmonics,[1–3] fuelled by the desire to exploit the associated enhancement of the electromagnetic near field for applications ranging from single-molecule sensing at visible frequencies[4,5] to cancer therapy in near infrared.[6] As localized particle plasmons are geometry-dependent resonances of the conduction electron sea of metallic nanostructures driven by the electromagnetic field, the spectral positions of these resonances depend sensitively on particle size and shape.[7] For particles of size $d \leqslant \lambda$, where λ is the wavelength of the impinging radiation, the plasmon mode has the character of an electric dipole, and for the noble metals gold and silver, its spectral position lies for sphere-shaped particles in a low permittivity environment in the visible part of the electromagnetic spectrum.[8,9]

Particularly, for applications in optical sensing and telecommunications, a controlled tunability of plasmon resonances throughout the visible and into the near-infrared spectral range is desirable. However, while it is well established that an increase in size of spherical or planar, disk-shaped nanostructures leads to redshifts of the respective dipole modes due to retardation effects, the concomitant increase in radiation damping[10] incurs a significant resonance broadening, therefore diminishing the total enhancement of the electromagnetic near field. A more promising approach lies in employing metal nanoparticles of geometries significantly deviating from spherical or disk-like shapes. Indeed, it has been shown that nanosized metallic rings sustain dipole-like resonances that can be tuned into the near-infrared region via a change in the width of the metallic ring,[11,12] while at the same time upholding the in-plane symmetry of the modes with regards to the polarization of the exciting light field. The reduced amount of metal compared to disks of equal size results in a decrease in absorption loss. Some line broadening with increasing outer diameter still occurs due to an increase in radiation damping; however, as we will show, this is significantly reduced compared to solid disks. Crucially, however, nanorings compare favorably to disks of the same size in the refractive index sensitivity of the dipolar plasmon frequency,[13] making this geometry superior for sensing applications. The same holds for crescent-shaped particles, which exhibit a lower radiation damping and therefore sharper resonances in the near infrared due to concentration of the plasmon mode into smaller volumes.[14]

Here, we discuss a related, conceptually simple system to achieve tunable, sharp plasmon resonances throughout the visible and near-infrared regimes. It consists of the concentric arrangement of a metallic nanoring with an embedded disk, separated from the inside wall of the ring by a small gap. The geometrical parameters of this ring/disk nanocavity are defined in Fig. 1. As will be shown below, the electric field of the fundamental modes of this cavity is highly con-

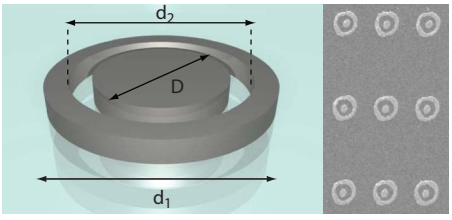

FIG. 1. (Color online) Geometry of the ring/disk cavity. The structure consists of a concentric arrangement of a nanoring (outer diameter d_1 and inner diameter d_2) and a central disk (diameter D). The height of the structure is h. The scanning electron microscope image shows an example of a 3×3 array of concentric ring/disk structures with $d_1 \approx 500$ nm fabricated using electron beam lithography and lift-off.

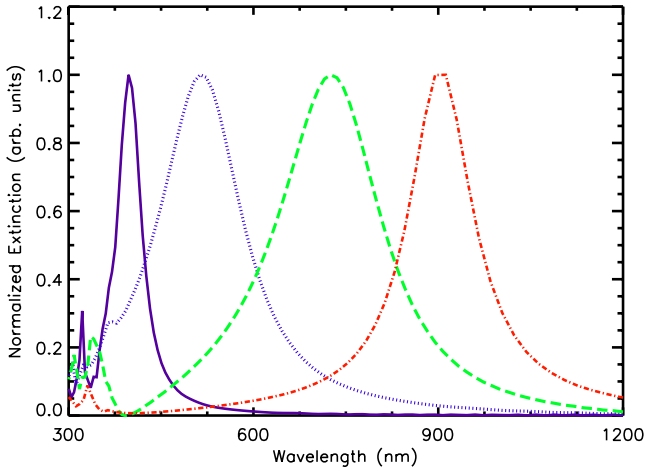

FIG. 2. (Color online) Normalized extinction spectra for cylindrical silver disks and rings of height $h=50$ nm surrounded by air, calculated using FDTD. The pulse is incident along the cylindrical axis of the disks/rings and polarized perpendicular to the axis. Purple (solid) and blue (dotted) lines are the extinction spectra for disks with $D=70$ nm and $D=140$ nm, respectively. The green (dashed) line is the extinction spectrum for a ring with $d_1=200$ nm and $d_2=100$ nm. The red (dash-dotted) line is for a ring with $d_1=200$ nm and $d_2=150$ nm.

fined in the gap between the ring and the disk, akin to subwavelength metal-insulator-metal slab waveguides.[15] For small slot sizes, therefore significantly higher field enhancement than for rings of same outer diameter can be achieved, while retaining in-plane polarization symmetry. Figure 1 also shows examples of structures fabricated using electron beam lithography with a dual-resist layer process on indium tin oxide glass slides and subsequent silver lift-off. In this paper, we focus on a computational investigation of the electromagnetic modes sustained by these systems, and details regarding fabrication and experimental characterization of single ring/disk nanocavities will be reported elsewhere.

For the analysis of this system, we use the finite-difference time-domain method (FDTD) to directly solve for the extinction spectrum of the ring-disk system. In order to gain an increased understanding into the nature of the fundamental electromagnetic resonances, we combine our results with plasmon hybridization theory,[16] which allows the identification of the resonances as bonding and antibonding hybrids of the fundamental ring and disk modes. This approach has already been successfully applied to the understanding of plasmon resonances in star-shaped particles.[17] To model the silver metal, we use a Drude model $\varepsilon(\omega)=\varepsilon_\infty-\frac{\omega_p^2}{\omega^2+i\omega\delta}$, with parameters $\varepsilon_\infty=4.039$, $\omega_p=1.390\,77\times10^{16}$ rad/s, and $\delta=3.139\,99\times10^{13}$ Hz. This fit provides an accurate description of the dielectric data of Ag in the wavelength regime of 300–2000 nm.[18] For the present relatively large structures, we do not need to include any size dependent additional damping.[19]

Starting with the fundamental building blocks of our hybridized system, Fig. 2 shows the calculated extinction spectra for representative silver disks and rings of height $h=50$ nm surrounded by air. The influence of a substrate layer will be discussed later on. For the moment, we limit our discussions to systems with sizes not exceeding an outer diameter of 200 nm. In this size interval, the dipolar resonance of an individual silver disk is tunable from around 400 nm to approximately 500 nm by increasing the disk diameter, which is accompanied by a notable peak broadening. The shorter wavelength features are higher order multipolar plasmons which can be excited because of retardation effects. For the rings, the plasmon resonances are bonding and antibonding combinations of primitive plasmon resonances associated with the inner and outer surfaces.[11] The major feature in each spectrum is the bonding dipolar ring resonance, while the short wavelength features also include weak antibonding ring modes. The plasmon resonance of a ring has a higher degree of tunability than the solid disk, since also the inner diameter can be varied,[11] leading to significant redshifts with decreasing ring wall size d_2-d_1. Another important property of the ring is that the width of its bonding plasmon resonance is reduced compared to that of a disk plasmon. For example, the full width at half maximum (FWHM) of the dipolar mode of a 400 nm diameter disk at 1033 nm is 1.09 eV, whereas the FWHM for the dipolar mode at 1796 nm for a ring of $d_2=400$ nm and $d_1=360$ nm is only 0.085 eV. This line shape narrowing is caused both by the reduction in radiation damping and by the decrease in electron-hole pair excitation rates for longer wavelengths.

FDTD is an intuitive computational technique providing real-time evolution pictures of the electromagnetic fields in the system under study. In our parallelized implementation,[20] a short Gaussian pulse composed of plane waves with frequency components in the spectral window of interest is directed into the simulation domain, in which electric and magnetic fields are updated using the standard FDTD algorithm.[21,22] A running-sum evaluation of the discretized Fourier transformation is performed to obtain the electric field distribution in the frequency domain. The divergence of the electric field is evaluated numerically to generate the amplitude of the charge distributions as a function of wavelength. The charge distributions so generated provide insight into the physical nature of the plasmon resonances shown in the extinction spectra. The extinction spectra are calculated by integrating the Poynting vector over the six surfaces of the simulation box and include the loss of electromagnetic energy both to absorption and scattering.[22]

In Fig. 3, we show the charge distribution amplitudes on several representative cross sectional surfaces of a ring and a disk in vacuum at the wavelengths of the major resonances. Panels (a)–(c) show the charge distribution amplitudes of a subwavelength cylindrical disk at its major resonance wavelength. Since plasmon modes can be described as incompressible deformations of the electron gas,[16,23] the only induced charges resides on the surfaces and are proportional to the amplitude of the plasmon. The force providing the restoring force for the plasmon oscillation originates from the electromagnetic interactions of these surface charges. The induced electric field is not localized only to the surface but penetrates also the metal for finite frequencies. The curves clearly show that the surface charges induced by the plasmon mode are largest on the top (and bottom) surfaces of the disk. The surface charges in the cut along the center of the struc-

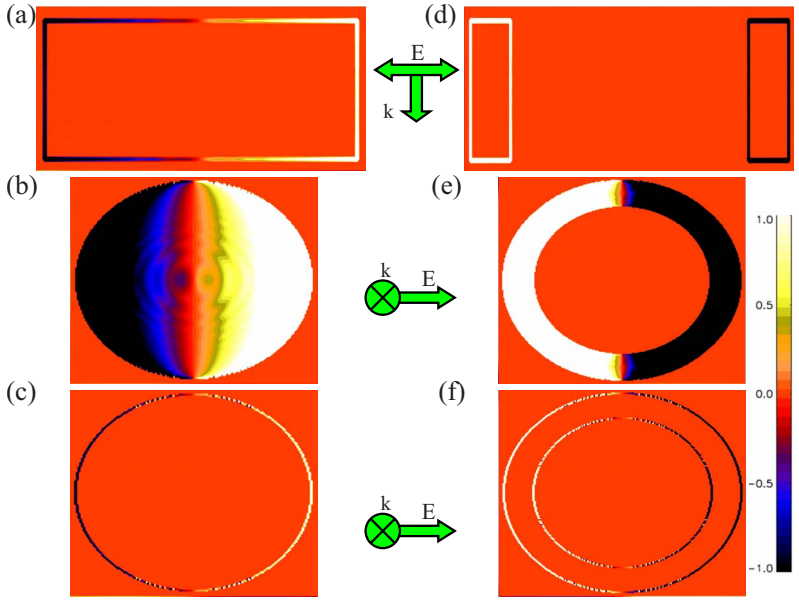

FIG. 3. (Color online) Charge distribution amplitudes for disks and rings in vacuum at their plasmon resonant frequencies in arbitrary units. Panels (a)–(c) are for a cylindrical disk with $D=140$ nm and $h=50$ nm. Panels (d)–(f) are for a cylindrical ring of same height and $d_1=200$ nm and $d_2=150$ nm. The resonance wavelengths are 515 nm for the disk (the blue line in Fig. 2) and 904 nm for the ring (the red line in Fig. 2). Panels (a) and (d) show the charge distribution on the surface cut along the cylinder axis. Panels (b) and (e) are for the top surface. Panels (c) and (f) are the center cross section of the disk/ring. The incident and polarization directions are denoted in the center of the graph.

tures are very small. An incompressible deformation of the conduction electron gas which primarily involves the electrons on the top and bottom surfaces has lower energy than a rigid displacement of the conduction electron distribution since the induced surface charges which provides the restoring force will be smaller. For a nanoring of similar size panels (d)–(f), the situation is similar, with charge distributions primarily induced on the top (and bottom) surfaces of the ring. The symmetric alignment of the surface charges on the inner and outer surfaces of the ring is a consequence of the incompressibility of the electron gas and results in the low energy bonding plasmon resonance analogous to the bonding dipolar nanoshell or thin film resonance.[23,24]

We now examine the plasmon resonances in the combined ring-disk nanocavity. Here, the plasmon modes are formed by hybridization of the primitive plasmons associated with the individual disk and the ring. As in a nanoshell or nanomatryushka,[23] the interactions between the primitive plasmons are determined by the separation between the surfaces of the metals and the relative energies of the primitive plasmons. In Fig. 4, we use the plasmon hybridization concept to analyze the nature of the two lowest energy plasmon resonances of the concentric ring-disk system of different interaction strengths. The panels show both the extinction spectrum of the particular structure at hand and the charge distributions amplitudes associated with the plasmon resonances. In each panel, the left and right boxes show the extinction spectra of the individual disk and ring constituents, respectively. The middle box in each panel shows the extinction spectrum for the interacting ring-disk systems. The dominant interactions resulting in the formation of the hybridized ring-disk plasmons are illustrated by the dotted lines. Panel (a) shows the plasmonic structure of a strongly interacting system with a 10 nm gap between the ring and the disk. The dipolar disk plasmon at 2.5 eV interacts both with the bonding dipolar ring resonance (BR) at 1.3 eV and the weaker antibonding dipolar ring resonance (AR) at 3.8 eV. The interactions results in several hybridized plasmon modes. The narrow resonance at 1 eV is a bonding resonance consisting of oppositely aligned individual disk and bonding ring dipolar plasmons (DBR). The net dipole moment of this resonance is smaller than those of the individual disk and and ring, resulting in less radiative damping and line narrowing as the mode becomes darker. The broader hybridized resonance at 2.2 eV is primarily a bonding combination of the primitive dipolar disk and the antibonding dipolar ring plasmon modes and will be referred to as the (DAR) mode. The corresponding antibonding resonance around 4 eV is indistinguishable because of the presence of other higher order modes and the strong damping at high energies. A close inspection of the charge density amplitude for the DAR resonance show that it also contains an antibonding admixture of the BR mode. However, to maintain the simplicity of Fig. 4, we do not illustrate this interaction.

As we increase the gap size from 10 to 15 nm [Fig. 4(b)], the interaction between the ring and the disk is weakened. The DBR mode (1.6 eV) is redshifted by 0.1 eV from the BR at 1.7 eV compared to the 0.3 eV redshift in Fig. 4(a). The DAR mode (2.5 eV) is redshifted by 0.6 eV from the dipolar disk mode at 3.1 eV. This is larger than the 0.3 eV redshift found for the small gap structure in panel (a). This is because the energy difference between the dipolar disk mode and the AR is much smaller in panel (b). When the gap between the ring and the disk is further enlarged to 40 nm, as shown in Fig. 4(c), the interactions become very small. The energy of the DBR mode 1.3 eV is approximately the same as the energy of the BR mode. The energy of the DAR is approximately the same as the dipolar disk mode, 3.1 eV. The optical response of the system is approximately equal to the sum of the optical spectra of the individual parts.

Metallic nanoring structures are promising substrates for surface enhanced raman spectroscopy (SERS) and localized surface plasmon resonance (LSPR) sensing applications because of their tunability and ability to provide large and spatially uniform field enhancements in the visible and near-IR regions. The reported electric field enhancement factor is

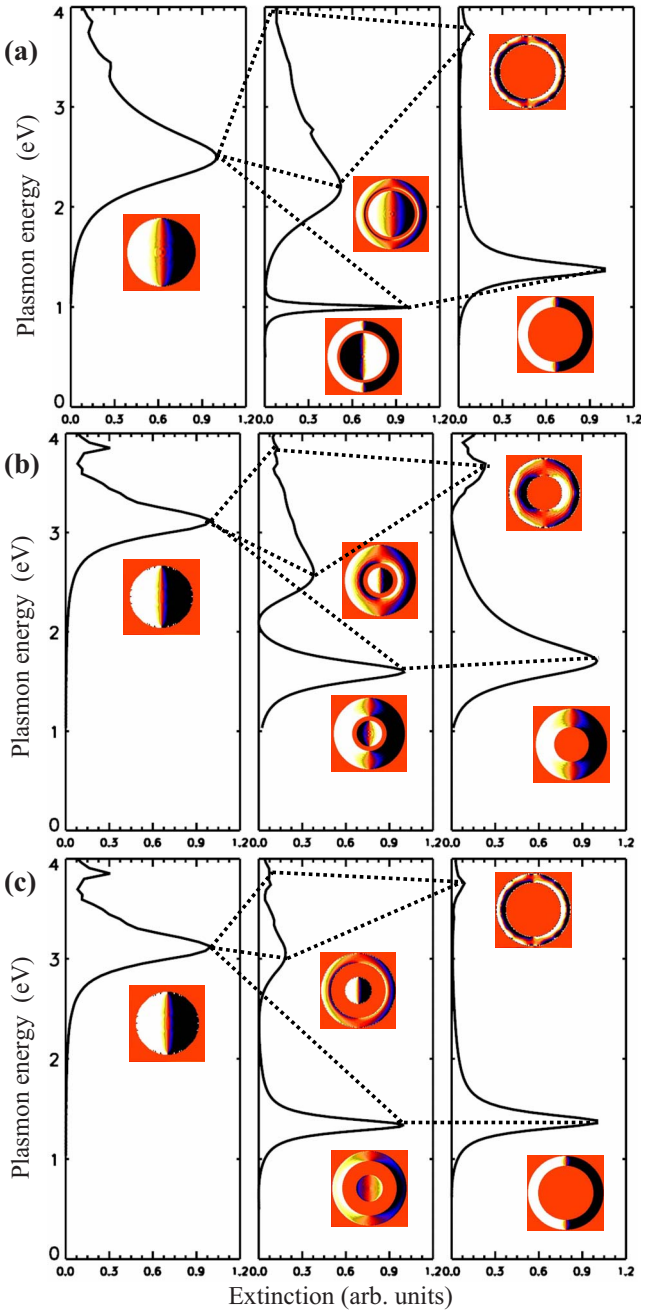

FIG. 4. (Color online) Hybridization diagram illustrating the nature of the plasmon resonances in concentric ring-disk structures. Panel (a) shows the strong hybridization in a system with d_1 =200 nm, d_2=150 nm, and D=130 nm. Panel (b) shows intermediate hybridization in a system with d_1=200 nm, d_2=100 nm, and D=70 nm. Panel (c) shows weak hybridization in a d_1=200 nm, d_2=150 nm, and D=70 nm. Left panels are the extinction spectra for individual disks as function of energy. Right panels are extinction spectra for the rings. The middle panels shows the spectra for the interacting system. The spectra of the individual disks have been multiplied by a factor of 6 to make them more visible in the figure. Black dotted lines illustrates some of the interactions that results in hybridized ring/disk plasmons. The charge distribution amplitudes associated with each spectral feature are shown next to the peaks.

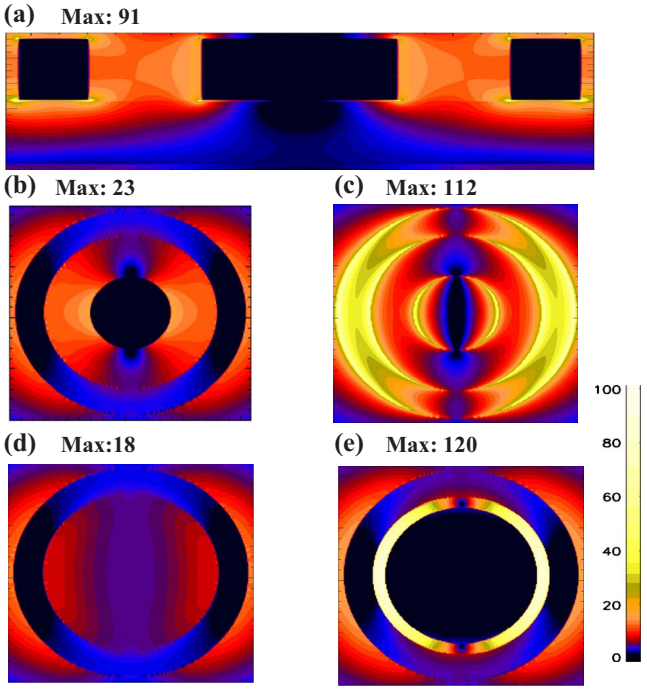

FIG. 5. (Color online) Contour plots of the electric field enhancement for ring and ring-disk systems on a silica substrate (permittivity of 2.04). Panels (a)–(c) show the electric field enhancement for a d_1=200 nm, d_2=150 nm, D=70 nm system at the resonance wavelength of 1032 nm. Panel (a) is a plane cut vertically along the axis of the ring and the disk. Panel (b) is a plane in the middle of the structure and panel (c) is along interface between the metal and substrate. Panel (d) shows the electric field enhancement on the middle cross section of a 200–150 nm ring on substrate at its resonance wavelength of 1009 nm. Panel (e) shows the electric field enhancement in the middle cross section of a ring-disk system of dimension d_1=200 nm, d_2=150 nm, and D=130 nm at the resonance wavelength of 1326 nm. All the ring/disks are with a height h=50 nm. On top of each panel is the maximum value of electric field enhancement in each plot.

about 8–10.[11,13] The addition of a disk in the center of the ring improves the functionality of the ring structure by both introducing additional tunability and by increasing the local electromagnetic field enhancements. In Fig. 5, we show the calculated field enhancements in two disk-ring systems on a silica substrate. The effect of the substrate is a small redshift of the plasmon resonances due to the screening charges induced at the interface between the metal and substrate. In Figs. 5(a)–5(c), the calculated electric field enhancements for the DBR mode for a 40 nm gap system are plotted on several cross sectional surfaces of the structures. For this large gap distance, the interaction between the ring and disk is very small [see Fig. 4(c)]. In spite of this, the resulting field enhancement of 23 in the center [Fig. 5(b)] is still larger compared to the field enhancement of 18 obtained for an individual ring on a substrate [Fig. 5(d)]. These numbers would be 23 and 12 if we only consider the electric field in the cavities which would be the part of the structure most accessible in a chemical sensing application. The electric field enhancement of the ring-disk structure is almost homoge-

neously distributed throughout the cavity, while for the ring, the electric field enhancements decrease rapidly toward the center of the ring. For a smaller gap such as 10 nm [Fig. 5(e)], the electric field enhancement is drastically increased to 120. This is around ten times larger than what is generated inside an individual ring. In Fig. 5(a), we show the electric field enhancement on a vertical cross section through the system. Because the surface charges are mainly distributed on the two ends of the ring/disk, the field enhancement could be about 90 on the top and bottom surfaces even for a 40 nm gap system. This property is illustrated more clearly in Fig. 5(c), where a maximum field enhancement of 112 is obtained along the substrate interface.

The fabrication of structures using high-resolution electron beam lithography and a negative resist process allows for gap sizes below 30 nm, which will be reported in a separate publication. As we will show now, hybridization effects become appreciably for even larger gaps if the size of the whole structure is scaled up. In Fig. 6, we calculate the extinction spectra for a larger ring-disk system. For an interacting system with a gap size of 50 nm, the DBR mode is appearing at the wavelength of 2121 nm. The relatively weak interaction still results in a appreciable redshift from the 1927 nm BR mode of the individual ring. The electric field enhancements is also increased by presence of the disk. On a surface across the middle of the structure, the field enhancement induced by the DBR mode is 43, while for the BR mode it is 28. As was the case for the disk-ring studied in Fig. 4(a), the reduced dipole moment of the DBR mode results in a reduction of the radiation damping. This results in a narrowing of the plasmon resonance from 0.081 eV for the BR mode to 0.055 eV for the DBR mode.

The strong tunability of the plasmon resonances of the proposed ring/disk structure makes it a promising substrate both as an LSPR sensor and for surface enhanced spectroscopies such as SERS. The possibility of tuning the plasmon resonances further into the infrared (Fig. 6) makes the structure particularly interesting as a substrate for surface enhanced infrared absorption. Although the field enhancements are not sufficiently strong for single molecule spectroscopy, the large sensing volume provided by the gap will enable many molecules to be probed which results in an increased signal.

In conclusion we have shown that the concentric ring/disk system represents a highly tunable metallic nanostructure capable of providing large electromagnetic field enhancements over a broad range of wavelengths extending from the visible into the infrared. The nature of the plasmon resonances can be understood simply as hybridization of the plasmon resonances associated with the individual disk and ring.

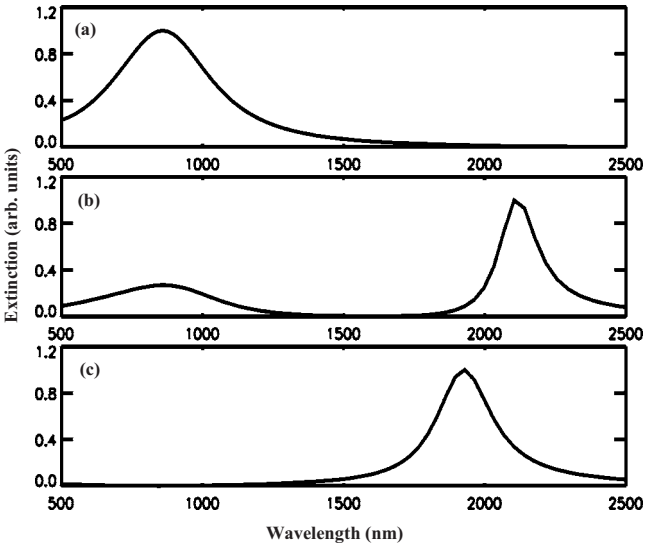

FIG. 6. Extinction spectra for a larger ring-disk system and its components on silica substrate. Panel (b) shows the extinction spectrum of a combined system with parameters of $d_1=400$ nm, $d_2=360$ nm, and $D=260$ nm. Panel (a) is only for the disk with diameter $D=260$ nm, and panel (c) is showing the extinction spectrum for the bare ring $d_1=400$ nm and $d_2=360$ nm. The height of the ring/disk is $h=50$ nm. The permittivity of silica used in the calculation is 2.04.

Charles de Nobriga is acknowledged for useful discussions. This material is based on work supported by the U.S. Army Research Laboratory and the U.S. Army Research Office under Contract No. W911NF-04-1-0203 (P.N. and H.F.), by the Robert A. Welch Foundation under Grant No. C-1222 (P.N.), by NSF under Grant Nos. EEC-0304097 and ECS-0421108 (P.N. and F.H.), and by the Engineering and Physical Sciences Research Council EPSRC (S.A.M.).

*nordland@rice.edu
†s.maier@imperial.ac.uk
‡Present address.

[1] S. A. Maier, *Plasmonics: Fundamentals and Applications*, 1st ed. (Springer, New York, NY, 2007).
[2] N. Halas, MRS Bull. **30**, 362 (2005).
[3] H. A. Atwater, Sci. Am. **296**, 56 (2007).
[4] K. Kneipp, H. Kneipp, I. Itzkan, R. R. Dasari, and M. S. Feld, J. Phys.: Condens. Matter **14**, R597 (2002).
[5] S. M. Nie and S. R. Emery, Science **275**, 1102 (1997).
[6] L. R. Hirsch, R. J. Stafford, J. A. Bankson, S. R. Sershen, B. Rivera, R. E. Price, J. D. Hazle, N. J. Halas, and J. L. West, Proc. Natl. Acad. Sci. U.S.A. **100**, 13549 (2003).
[7] J. Zhu, J. Nanosci. Nanotechnol. **7**, 1059 (2007).
[8] G. Mie, Ann. Phys. **25**, 377 (1908).
[9] B. N. Khlebtsov and N. G. Khlebtsov, J. Quant. Spectrosc. Radiat. Transf. **106**, 154 (2007).
[10] A. Wokaun, J. P. Gordon, and P. F. Liao, Phys. Rev. Lett. **48**, 957 (1982).
[11] J. Aizpurua, P. Hanarp, D. S. Sutherland, M. Käll, G. W. Bryant, and F. J. Garcia de Abajo, Phys. Rev. Lett. **90**, 057401 (2003).
[12] J. Aizpurua, L. Blanco, P. Hanarpo, D. S. Sutherland, M. Kall, G.

W. Bryant, and F. J. G. de Abajo, J. Quant. Spectrosc. Radiat. Transf. **89**, 11 (2004).
[13] E. M. Larsson, J. Alegret, M. Käll, and D. S. Sutherland, Nano Lett. **7**, 1256 (2007).
[14] R. Bukasov and J. S. Shumaker-Parry, Nano Lett. **7**, 1113 (2007).
[15] J. A. Dionne, H. J. Lezec, and H. A. Atwater, Nano Lett. **6**, 1928 (2006).
[16] E. Prodan, C. Radloff, N. J. Halas, and P. Nordlander, Science **203**, 419 (2003).
[17] F. Hao, C. L. Nehl, J. H. Hafner, and P. Nordlander, Nano Lett. **7**, 729 (2007).
[18] P. B. Johnson and R. W. Christy, Phys. Rev. B **6**, 4370 (1972).
[19] C. L. Nehl, N. K. Grady, G. P. Goodrich, F. Tam, N. J. Halas, and J. H. Hafner, Nano Lett. **4**, 2355 (2004).
[20] C. Oubre and P. Nordlander, J. Phys. Chem. B **108**, 17740 (2004).
[21] D. M. Sullivan, *Electromagnetic Simulation Using the FDTD Method* (IEEE, Piscataway, NJ, 2000).
[22] A. Taflove and S. C. Hagness, *Computational Electrodynamics: The Finite-Difference Time Domain Method* (Artech House, Norwood, MA, 2000).
[23] E. Prodan and P. Nordlander, J. Chem. Phys. **120**, 5444 (2004).
[24] F. Le, N. Z. Lwin, N. J. Halas, and P. Nordlander, Phys. Rev. B **76**, 165410 (2007).